



Coulombically-stabilized oxygen hole polarons enable fully reversible oxygen redox

Journal:	<i>Energy & Environmental Science</i>
Manuscript ID	EE-ART-04-2021-001037.R1
Article Type:	Paper
Date Submitted by the Author:	20-Jun-2021
Complete List of Authors:	<p>Abate, Iwnetim; Stanford University, Materials Science and Engineering; SLAC National Accelerator Laboratory, Stanford Institute for Materials & Energy Sciences</p> <p>Pemmaraju, C. Das ; SLAC National Accelerator Laboratory, Stanford Institute for Materials & Energy Sciences</p> <p>Kim, Se Young; University of Waterloo Faculty of Science, Chemistry Department</p> <p>Hsu, Kuan ; Stanford University, Department of Materials Science and Engineering</p> <p>Sainio, Sami ; SLAC National Accelerator Laboratory, Stanford Synchrotron Radiation Light source</p> <p>Moritz, Brian; SLAC National Accelerator Laboratory, Stanford Institute for Materials & Energy Sciences</p> <p>Vinson, John; National Institute of Standards and Technology,</p> <p>Toney, Michael; University of Colorado at Boulder,</p> <p>Yang, Wanli; Lawrence Berkeley National Laboratory, Advanced Light Source</p> <p>Gent, William; Stanford University, Department of Materials Science and Engineering</p> <p>Deveraux, Thomas; Stanford University and SLAC National Accelerator Laboratory, Stanford Institute for Materials and Energy Sciences</p> <p>Nazar, Linda; University of Waterloo, Chemistry</p> <p>Chueh, William; California Institute of Technology, Materials Science</p>

Coulombically-stabilized oxygen hole polarons enable fully reversible oxygen redox

Iwnetim I. Abate^{1,2}, C. Das Pemmaraju², Se Young Kim³, Kuan H. Hsu¹, Sami Sainio⁴, Brian Moritz², John Vinson⁵, Michael F. Toney^{1,4}, Wanli Yang⁶, William E. Gent¹, Thomas P. Devereaux^{1,2*}, Linda F. Nazar^{3*}, William C. Chueh^{1,2*}

¹Department of Materials Science and Engineering, Stanford University, 496 Lomita Mall, Stanford, CA 94305, USA.

²Stanford Institute for Materials & Energy Sciences, SLAC National Accelerator Laboratory, 2575 Sand Hill Road, Menlo Park, CA 94025, USA.

³Department of Chemistry and the Waterloo Institute for Nanotechnology, University of Waterloo, 200 University Avenue West, Waterloo, Ontario N2L 3G1, Canada.

⁴Stanford Synchrotron Radiation Light source, SLAC National Accelerator Laboratory, 2575 Sand Hill Road, Menlo Park, CA 94025, USA.

⁵Material Measurement Laboratory, National Institute of Standards and Technology, Gaithersburg, Maryland 20899, USA.

⁶Advanced Light Source, Lawrence Berkeley National Laboratory, Berkeley, CA 94720, USA.

*email: tpd@stanford.edu (T.P.D.), lfnazar@uwaterloo.ca (L.F.N.), wchueh@stanford.edu (W.C.C.)

Abstract

Stabilizing high-valent redox couples and exotic electronic states necessitate an understanding of the stabilization mechanism. In oxides, whether they are being considered for energy storage or computing, highly oxidized oxide-anion species rehybridize to form short covalent bonds and are related to significant local structural distortions. In intercalation oxide electrodes for batteries, while such reorganization partially stabilizes oxygen redox, it also gives rise to substantial hysteresis. In this work, we investigate oxygen redox in layered $\text{Na}_{2-x}\text{Mn}_3\text{O}_7$, a positive electrode

material with ordered Mn vacancies. We prove that coulombic interactions between oxidized oxide-anions and the interlayer Na vacancies can disfavor rehybridization and stabilize hole polarons on oxygen (O^-) at 4.2 V vs. Na/Na⁺. These coulombic interactions provide thermodynamic energy saving as large as O-O covalent bonding and enable ~40 mV voltage hysteresis over multiple electrochemical cycles with negligible voltage fade. Our results establish a complete picture of redox energetics by highlighting the role of coulombic interactions across several atomic distances and suggest avenues to stabilize highly oxidized oxygen for applications in energy storage and beyond.

Introduction

Stable and reversible high-valent redox couples are foundational to (electro)chemical and catalytic transformations. A prominent application of such redox couples is intercalation battery electrodes.¹ In particular, the phenomenon of anionic redox in lithium- and sodium-ion positive electrodes has the potential to significantly improve cell energy density by providing additional high voltage capacity beyond that of most transition metal (TM) redox couples.²⁻⁴ Two major hypotheses have guided the search for intercalation layered oxides with stable and reversible oxygen redox. First, short covalent bonding between oxygen atoms (e.g., ~1.5 Å O–O peroxy, vs. 2.8 Å in a typical TMO_6 octahedron)⁴⁻⁶ and between TM and oxygen atoms (e.g., ~1.8 Å metal-oxo vs. 2.0 Å typical)⁷ can stabilize oxidized oxide species against oxygen release. Second, the energetic penalty associated with the local distortion induced by such major bonding rearrangements can be mitigated by in-plane⁸ and out-of-plane metal vacancy/antisite disorder^{5,7,9,10} (i.e., so-called cation migration), leading to overall energy savings. The convergence of these two ideas has led to the current paradigm that oxygen redox and cation disordering come hand-in-hand to achieve stable but hysteretic redox in battery electrodes, typically involving hysteresis of several hundred mV.¹⁰⁻¹² As such, efforts have been directed at minimizing the hysteresis associated with transition metal migration,¹² as well as identifying new structures that can accommodate local distortions induced by anion redox without disorder.¹ An alternative approach is to avoid such restructuring all together and therefore mitigate hysteresis.

Recently, several groups reported an anionic redox active material, $\text{Na}_{2-x}\text{Mn}_3\text{O}_7$, with a very small voltage hysteresis (~ 60 mV).¹³⁻¹⁶ The negligible hysteresis is maintained even upon deep deintercalation unlike other materials where the magnitude of voltage hysteresis scales with the extent of deintercalation.¹⁷ However, the mechanism that allowed such remarkable performance is still unclear. For example, Yamada and colleagues observed the emergence of a new absorption feature at ~ 531 eV upon anionic redox in X-ray absorption spectroscopy (XAS) measurements,¹³ a feature resulting from a redox mechanism typical in oxygen-redox electrodes with large voltage hysteresis, such as $\text{Li}_{1+x}\text{Ni}_{1-y-z}\text{Mn}_y\text{Co}_z\text{O}_3$ (NMC),¹⁰ $\text{Li}_{2-x}\text{Ir}_{1-y}\text{Sn}_y\text{O}_3$,⁷ and $\text{Na}_{0.75}\text{Li}_{0.25}\text{Mn}_{0.75}\text{O}_2$.⁹ However, since $\text{Na}_{2-x}\text{Mn}_3\text{O}_7$ and the other electrode materials exhibit differing hysteresis, a distinctive redox mechanism and therefore XAS features would be expected. Therefore, an understanding of the redox mechanism in $\text{Na}_{2-x}\text{Mn}_3\text{O}_7$ could inform ways we can achieve similar exceptional behavior in other Na and Li based oxide positive electrode materials.

In this work, we report unambiguous experimental and computational spectroscopic confirmation of a redox mechanism in $\text{Na}_{2-x}\text{Mn}_3\text{O}_7$ that is different from anionic redox positive electrode materials with high-hysteresis. We reveal oxygen hole polaron (O^-) formation and its electrochemical redox stability upon charging. The persistent ordered Mn vacancies in this electrode material provides the basis for calculating and understanding redox energetics in the absence of metal cation disordering. A clear picture for oxygen redox emerges: electrostatic interactions between oxygen hole polarons and Na vacancies compete with covalent bonding and transition metal disorder to determine the redox pathway. Through this understanding, we demonstrate that coulombic interactions can stabilize the otherwise unstable oxygen holes and provide energy saving as much as O-O covalent bonding, achieving exceptionally low, ~ 40 mV voltage hysteresis over electrochemical cycling with negligible voltage fade. Beyond batteries, stabilizing unusual polaronic states has many implications for defect engineering in materials for energy storage systems.

Results and discussion

Structurally, one out of every seven Mn sites are vacant in the TM layer of $\text{Na}_{2-x}\text{Mn}_3\text{O}_7$ ($\text{Na}_{4/7-x}\text{Mn}_{6/7}\square_{1/7}\text{O}_2$ where \square = vacant sites in the TM layer) (Fig. 1A). This results in two oxygen sublattices: oxygen anions with two Mn neighbors (O-Mn2, termed “O1”) and oxygen anions with three Mn neighbors

(O-Mn3, termed “O2”). The substantial difference in ionic radii between octahedral Mn^{IV} (0.53 Å) and Na^I (1.02 Å) and the large interlayer spacing further increases the penalty for antisite defects. Previous works showed low-voltage hysteresis by charging up to 4.7 V.^{13–15} However, voltage and capacity fading is observed above 4.4 V vs Na/Na⁺, possibly due to side reactions and electrolyte decomposition (Fig. 1B and C). Since we are interested in determining the exact anionic redox mechanism, we cycled the material in the voltage region where electrolyte decomposition and surface Mn oxidation are minimal (fig. S1). Figure 1D shows the reversible electrochemistry of Na_{2-x}Mn₃O₇ between X = 0 and ~ 0.5 (25% desodiation) over 30 cycles at a C/20 rate between 3.5 V and 4.3 V vs Na/Na⁺, where C is 166 mA g⁻¹. The symmetric and overlapping profiles of the differential capacity curve (Fig. 1D inset) further confirms reversibility of the redox process and absence of voltage fade in the voltage plateau region. This plateau centered at 4.17 V has been attributed to de/intercalation of the octahedrally coordinated Na₂ ions.¹⁴ The Na₁ ions that occupy trigonal prismatic sites in the layers above and below the Mn vacancies (Fig. 1A) are retained in this process, but extracted on the higher voltage plateau (Fig. 1B). Importantly, the electrode exhibits a low voltage hysteresis of ~40 mV between charge and discharge, smaller by several factors than that reported in other known Li- and Na-based anionic-redox-active electrodes.^{9–11} The voltage hysteresis remains largely constant with cycling (fig. S2).

The crystal structure is stable up to 4.3 V with < 0.5 Na remaining in the interlayer gap, unlike other Na layered TM oxides employing high-valent redox, such as α -NaFeO₂.¹⁸ Structural stability over repeated redox cycles was confirmed by synchrotron powder X-ray diffraction (XRD, Fig. 1E) and Mn K-edge extended X-ray absorption fine structure (EXAFS, Fig. 1F). The Fourier-transformed EXAFS spectra, shown in Fig. 1F, reveal that a slight increase in the Mn-O bond length (< 2%) is the only local structural change upon charging to 4.3 V. This indicates that the bond order does not change significantly upon oxidation. Likewise, there is negligible change in the pre-edge feature in the Mn K-edge X-ray absorption spectrum, proving the absence of Mn migration to tetrahedral sites and the stability of the local structure (fig. S3D). The negligible changes in the FWHM of the XRD reflection at low angle (Fig. S3C) and the

invariant XRD patterns shown through the 10th cycle (Fig. 1E) indicate structural stability that is consistent with previous reports.^{13–15}

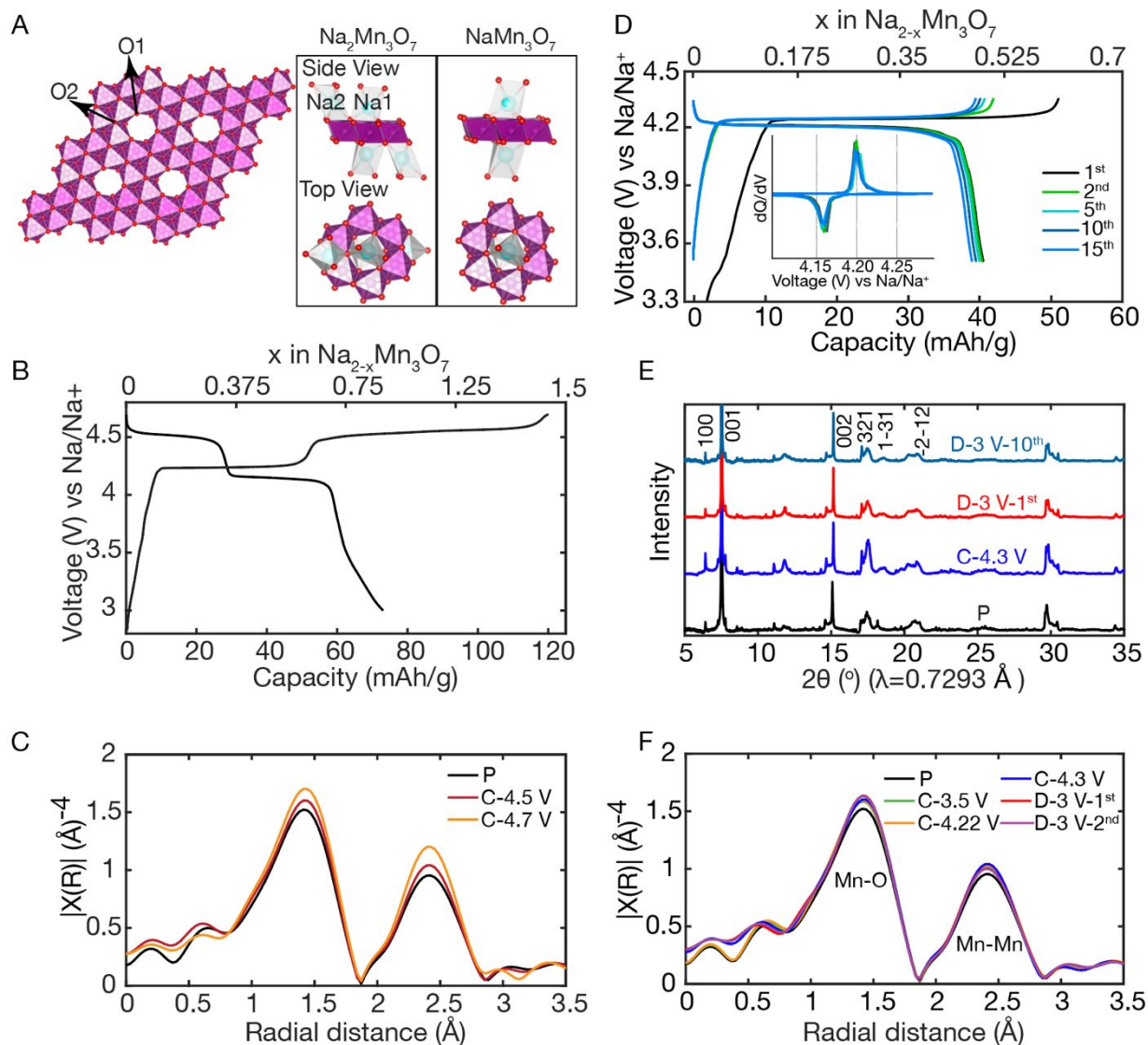


Fig. 1. Reversible electrochemistry and stable structure. (A) Structure of the Mn-O layer in Na₂Mn₃O₇ (Mn atoms shown in magenta and O atoms in red). One out of seven Mn sites are vacant, which creates two unique O environments: O-Mn2 (O1) in the ring surrounding the Mn vacancy; and O-Mn3 (O2). Top and side view of pristine and charged state. There are two sodium sites: Na2 (distorted octahedral) and Na1 (prismatic). (B) Voltage versus specific capacity at C/20 between 2.7 V and 4.7 V. We observed voltage and capacity fading upon cycling for several cycles when charging to 4.7 V. Similar to Li-excess materials, we believe that it is due to oxygen gas release from the particle surface.¹⁹ In addition, as 4.7 V is at the edge of the stability window of the electrolyte (Fig. S1), side reactions that will contribute to capacity fade are also expected. (C) Fourier transform of the ex-situ EXAFS spectra taken at the same voltage conditions. The negligible change in the EXAFS profile indicates preservation of the local structure upon deep desodiation. (D) Voltage profile up to the 15th cycle at C/20 (theoretical (de)intercalation of 2 Na⁺ per Na₂Mn₃O₇ in 20 h) between 3.5 V - 4.3 V vs Na/Na⁺, with very low voltage hysteresis (~40 mV). Inset: differential

capacity as a function of voltage (dQ/dV vs V). (F) Synchrotron powder X-ray diffraction of the pristine material; electrodes were charged to 4.3 V in the 1st cycle and discharged to 3 V at the 1st and 10th cycle (D-3V-1st and D-3V-10th). The XRD patterns exhibit negligible changes, indicating minimal structural modification upon cycling and fig. S3 shows the FWHM of the (100) reflection remains constant. (F) Fourier transform of the ex-situ EXAFS spectra of the pristine material (P) and electrodes charged to 3.5 V, 4.22 V, and 4.3 V in the 1st cycle and discharged to 3 V in the 1st and 2nd cycle (D-3V-1st and D-3V-2nd), respectively. The first peak corresponds to Mn-O distances and the second to Mn-Mn distances; data are not corrected for scattering phase shift. The negligible change in the EXAFS profile indicates preservation of the local structure upon cycling.

To elucidate the nature of this highly reversible redox couple in $\text{Na}_{2-x}\text{Mn}_3\text{O}_7$, we performed X-ray absorption spectroscopy (XAS) at the O K -edge (Fig. 2) and at the Mn L - and K -edges (fig. S4-5). From total electron yield XAS, we confirmed a slight oxidation on the surface where we estimated the Mn oxidation state to change from $\sim +3.9$ in the pristine state to $\sim +4.0$ upon charging, fig. S4. This minimal oxidation contributes to the capacity only up to ~ 4.2 V (in the sloping region of the voltage curve). Both Mn K and L -edge spectra do not change during the voltage plateau. Rather, the plateau capacity at ~ 4.2 V arises from the oxidation of oxygen anions. The O K -edge resonant inelastic x-ray scattering (RIXS) map, Fig. 2A, shows the emergence of a new feature at an excitation energy of ~ 527.5 eV upon charging, which disappears on discharge. This new feature also appears in the XAS at the same energy as shown in Fig. 2B and linearly increases in intensity upon anionic redox. The lack of change in the Mn K -edge (fig. S5) indicates that bulk Mn redox does not contribute to the capacity. Crucially, the oxygen redox feature remains largely constant in magnitude and reproducible between the 1st and 10th cycle (Fig. 2C), directly confirming the reversibility of this oxygen redox couple. Upon deep desodiation up to 4.7V (50% desodiation) (Fig. 2D), we observed increase in the intensity of the ~ 527.5 eV peak, unlike previous reports.¹³ The increase of the ~ 527.5 eV peak intensity during charging from 4.5 V to 4.7 V indicates that the concentration of localized holes increases because of their continuous generation upon anionic redox, as we expect. This also suggests that the anionic redox mechanism below 4.5 V is the same as above 4.5 V as we elucidate below.

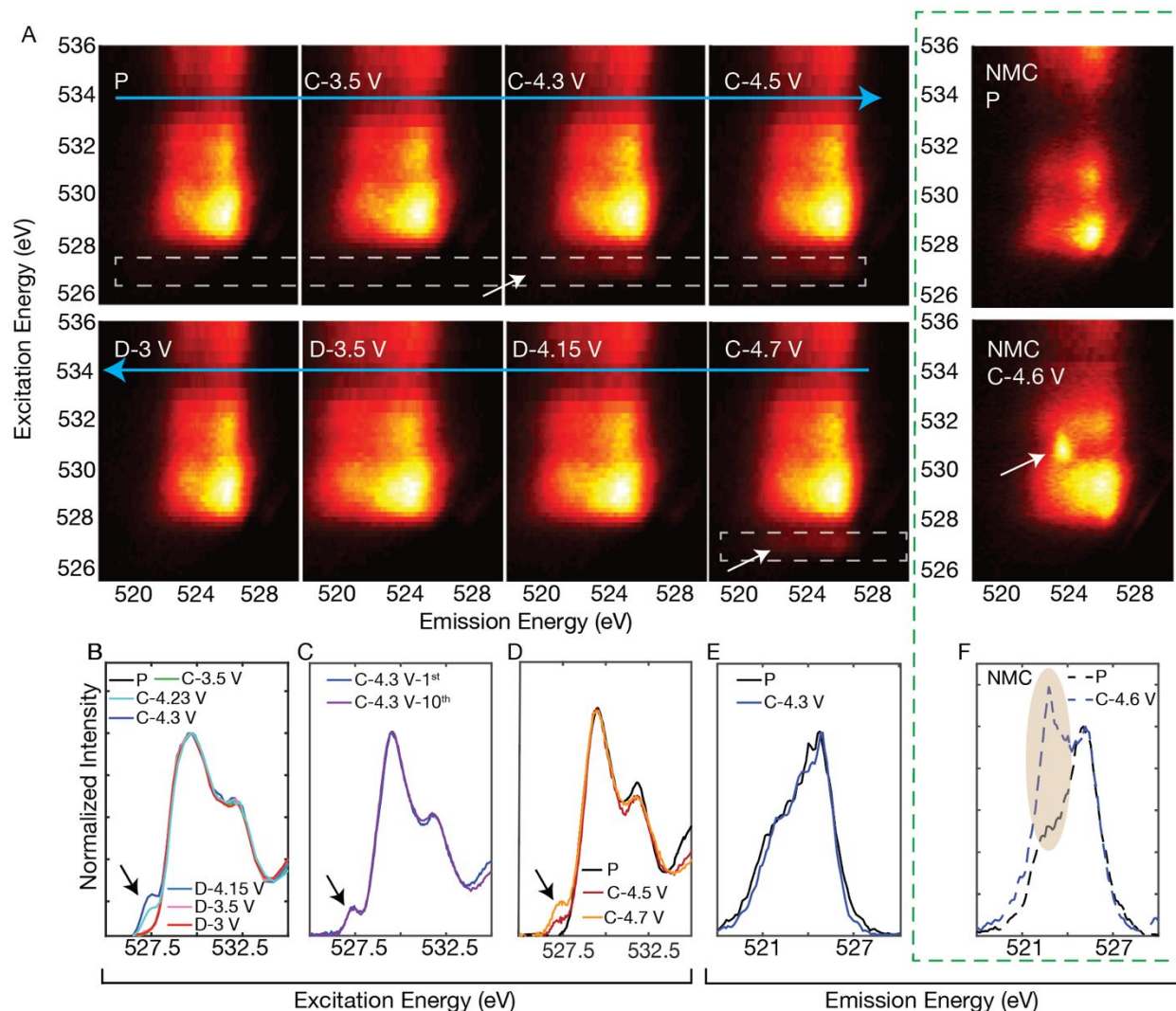


Fig. 2. Oxygen-redox in $\text{Na}_{2-x}\text{Mn}_3\text{O}_7$. (A) O K-edge RIXS maps of $\text{Na}_{2-x}\text{Mn}_3\text{O}_7$ from pristine to 4.7 V during charging (P to C-4.7 V) and from 4.15 V to 3 V during discharging in the bottom panel (D-4.15 V to D-3 V). The anionic-redox feature emerges at an excitation energy of ~ 527.5 eV upon charging (4.25-4.7 V) as indicated by the white arrow. O K-edge RIXS maps of pristine and charged LR-NMC ($\text{Li}_{1.17-x}\text{Ni}_{0.21}\text{Co}_{0.08}\text{Mn}_{0.54}\text{O}_2$) are also shown for comparison (NMC-P and NMC-4.6 V). The anionic-redox feature emerges at an excitation energy of ~ 531 eV upon charging (4.6 V) as indicated by the white arrow. All maps are taken during the first cycle. (B) O K-edge XAS spectra of $\text{Na}_{2-x}\text{Mn}_3\text{O}_7$, taken at the same voltage conditions as in panel A, showing the emergence of the peak at ~ 527.5 eV. (C) Comparison of the O K-edge XAS after charging (4.3 V) for the 1st and the 10th cycle. The normalized intensity of the ~ 527.5 eV feature is equivalent for the two spectra, indicating the stability of the anionic-redox mechanism. (D) O K-edge XAS of $\text{Na}_{2-x}\text{Mn}_3\text{O}_7$ from pristine to 4.7 V during charging (P to C-4.7 V). The increase in the intensity of the 527.5 eV peak when charging between 4.5 V and 4.7 V indicates that anionic redox with a similar mechanism takes place on the ~ 4.3 V and ~ 4.5 V plateau. Emission spectra obtained by integrating the RIXS maps along a cut at ~ 531 eV excitation energy to investigate the presence of O-O dimers in $\text{Na}_{2-x}\text{Mn}_3\text{O}_7$ (E) & NMC (F). A peak at 523 eV (shaded region) from such a line cut has been assigned previously to O-O dimer formation.^{7,10} The absence of this peak in $\text{Na}_{2-x}\text{Mn}_3\text{O}_7$ indicates a lack of dimer formation.

The spectroscopic signature of oxygen redox in $\text{Na}_{2-x}\text{Mn}_3\text{O}_7$ is distinct from a vast majority of known anion-redox-active electrodes. For example, NMC,¹⁰ $\text{Li}_{2-x}\text{Ir}_{1-y}\text{Sn}_y\text{O}_3$,⁷ and $\text{Na}_{0.75}\text{Li}_{0.25}\text{Mn}_{0.75}\text{O}_2$ ⁹

share the same spectroscopic signature in XAS or RIXS (~ 531 eV feature in XAS or a sharp feature at 531 eV excitation energy and 523 eV emission energy in RIXS, Fig. 2A for NMC). As can be seen in Figure 2D and E, such a feature is absent in $\text{Na}_{2-x}\text{Mn}_3\text{O}_7$. In electrodes with a 523 eV emission energy feature, the substantial structural disorder and large voltage hysteresis upon anionic redox has been linked to the formation of ~ 1.5 Å O-O dimers, which was proposed through comparison with a library of peroxide reference compounds using RIXS¹ and Raman spectroscopy although the precise speciation is still under debate.^{20–22} The absence of a peak at ~ 800 cm^{-1} in the Raman spectrum of $\text{Na}_{2-x}\text{Mn}_3\text{O}_7$ (fig. S6) indeed shows that 1.5 Å O-O peroxo moieties do not form.²⁰ We note that $\text{Na}_{0.6}\text{Li}_{0.2}\text{Mn}_{0.8}\text{O}_2$ ⁹ exhibits both the RIXS feature corresponding to O-O as well as the feature at an excitation energy of 527.5 eV observed in this work. However, as would be expected in an electrode material exhibiting oxygen dimerization, it exhibits a large voltage hysteresis and significant voltage fade.

Next, we performed *ab-initio* calculations using density-functional theory (DFT) with the Heyd–Scuseria–Ernzerhof functional, one of the better performing functionals for the ground state, and the Bethe–Salpeter Equation (BSE), a state-of-the art method for the excited state to understand the spectroscopic signature and energetic stability of oxidized oxide species. While it is challenging to employ first-principles calculations to identify the lowest energy structure of disordered materials (especially in the oxidized state), $\text{Na}_{2-x}\text{Mn}_3\text{O}_7$'s structural robustness against disordering makes it ideal for accurate first-principles analysis. Figure 3A shows a schematic top view of the pristine structure (sodium atoms colored cyan), with the corresponding density-of-states (DOS) shown in Fig. 3B. The two oxygen sublattices, “O1” and “O2” (Fig. 1A) exhibit a very different contribution to the DOS. Close to the Fermi level, the relative atomic contribution to the density-of-states follows the order $\text{O1} > \text{Mn} > \text{O2}$. Desodiation (charging) involves the preferential participation of the O1 species.

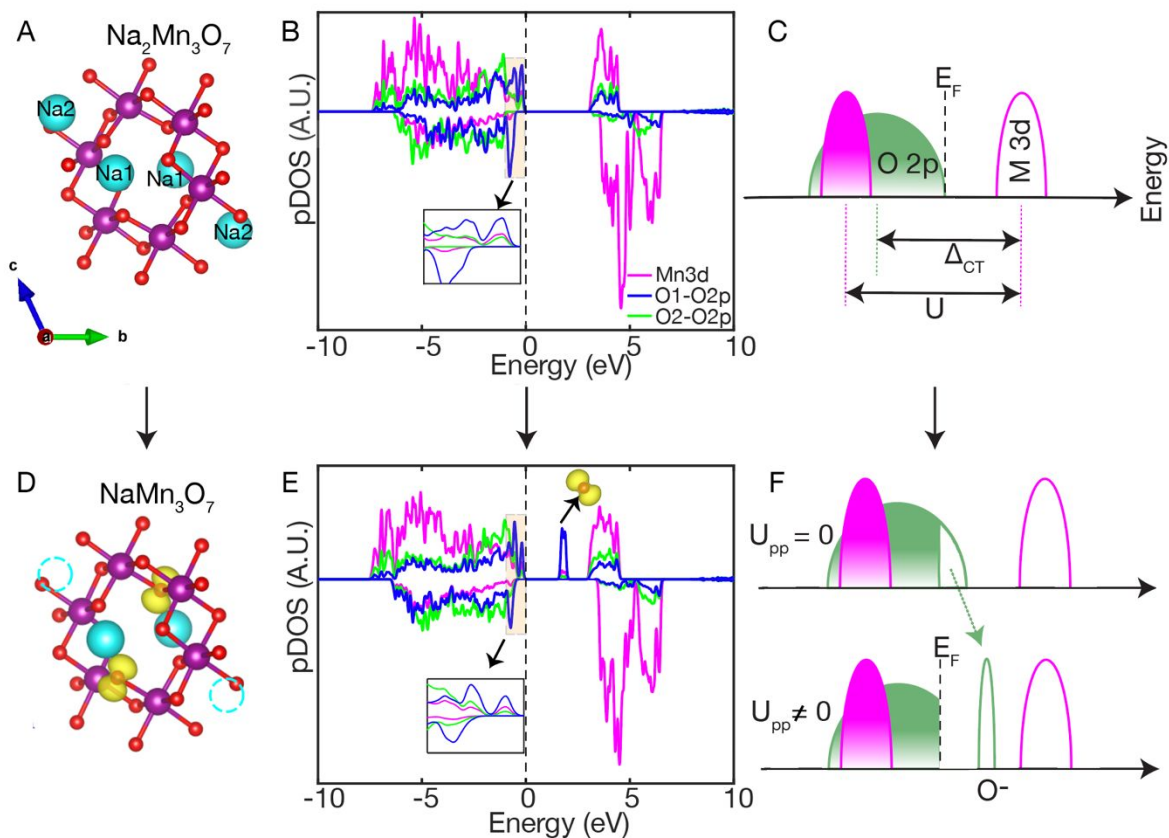


Fig. 3. Density of states (DOS) of $\text{Na}_{2-x}\text{Mn}_3\text{O}_7$ from DFT. (A) Structure in the pristine state (Na atoms in cyan). (B) Local DOS showing that O-2p states dominate the band near the Fermi level, with O1 oxygen (blue, O1-2p) having a larger contribution to the DOS near the Fermi level than O2 oxygen (green, O1-2p). Inset shows the DOS near the Fermi level. (C) Based on the Zaanen–Sawatzky–Allen (ZSA)²³ classification, $\text{Na}_{2-x}\text{Mn}_3\text{O}_7$ is a charge transfer insulator with the oxygen 2p band closer to the Fermi level than the metal (Mn) 3d band (Fig. 3C). Here, $U > \Delta_{\text{CT}}$, where U is the coulomb interaction energy for the 3d Mn electrons and Δ_{CT} is the charge transfer energy. (D) Structure after charging (desodiation, $\text{Na}_1\text{Mn}_3\text{O}_7$), with hole polarons on oxygen (spin density shown in yellow dumbbells), which form on the O1 species near the removed sodium atomic positions. In this work, the spin density of the hole polarons depicted is calculated over an energy range spanning the single particle level in the band gap associated with the species. (E) Local DOS in the charged (desodiated) state, where hole polarons localize on O1 atoms to form in-gap states. Inset shows the DOS near the Fermi level. (F) DOS schematic of charged state (NaMn_3O_7). Localized hole states form mid-gap states.

We simulated desodiated NaMn_3O_7 in the ground state by removing Na from the octahedral sites, and examined multiple configurations with holes localized on O1 and O2. Localized holes on O2 sites could not be realized following DFT self-consistent field iterations, suggesting that such a configuration is not a metastable state of the desodiated system. Instead, we find holes are localized on the under-coordinated O1 sites that surround the structural Mn vacancy (Fig. 3D). The local environment of O1 satisfies the condition for oxygen redox proposed by Seo et al.²⁴ First, we present results on the oxidation of two O1 located on

opposite ends of the oxygen network surrounding a Mn vacancy (we term this the third-nearest neighbor, 3NN, configuration). The Mn-O1 bond length increases slightly, by $< 2\%$ (consistent with EXAFS, fig. S3). Projected density of states indicates that oxidation localizes and upshifts the O $2p$ state at the top of the valence state by 1.4 eV (Figs. 3E & F), confirming that state corresponds to an oxygen hole polaron (O^-). We attribute the peak appearing at ~ 527.5 eV in the O K -edge XAS and RIXS to this localized hole polaron. Further confirmation is provided in the next section.

Next, we theoretically model the O K -edge XAS spectra using BSE method.^{25,26} As shown in Figs. 4A and 4B, the experimentally-observed spectra in Fig. 2 are well reproduced. We can now assign the spectral features to O1 and O2. In the pristine material (Fig. 4A), the main XAS peak at 529.5 eV is attributed to equal contributions from O1 (blue) and O2 (green), corresponding to the $O_{1s} \rightarrow (Mn_{3d}-O_{2p}^*)$ transitions. However, in the desodiated state (Fig. 4B), the peak at 527.5 eV arises from localized hole polarons (O^-) that form almost exclusively on O1 oxygen sites as shown in more detail in the inset of fig. S7 and Fig. 4B at 25% and 50% of desodiation, respectively. In general, these observations are in excellent agreement with the experimental XAS and RIXS results, as well as the projected DOS obtained from DFT.

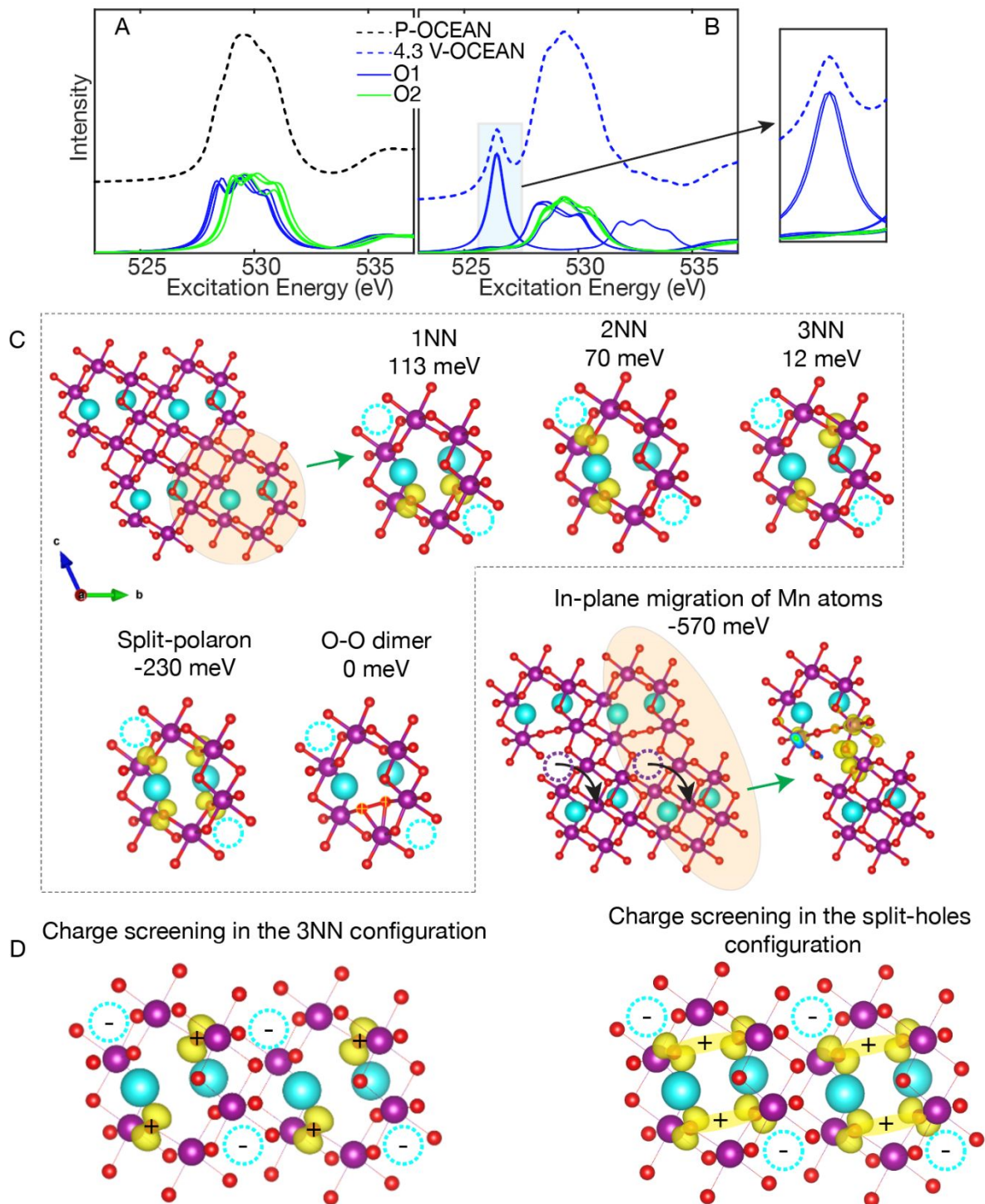


Fig. 4. Confirmation via XAS simulation and O^- species stabilization mechanism. (A) & (B) Simulated O K-edge XAS for pristine and charged samples (50% desodiation, $\text{Na}_1\text{Mn}_3\text{O}_7$), respectively. There are 7 O1 atoms and 7 O2 atoms in the unit cell. The 7 blue solid lines are for the O1 atoms and the 7 green solid lines are for O2 atoms. The sum of these spectra are shown for pristine (black dotted curve, $\text{Na}_2\text{Mn}_3\text{O}_7$) and charged (blue dotted curve, NaMn_3O_7). The dominant peak ~ 529.5 eV is from both O1 and O2 species; however, the O1 atoms have an out-weighted contribution to the localized hole polaron, which gives rise to the peak at ~ 527.5 eV. (C) Comparing the

energy (per Na atom removed) of different oxygen hole configurations. The split-polaron configuration (where a hole is shared among two O1 atoms) is the most stable configuration compared to first, third nearest neighbor (1NN & 3NN) and peroxo configurations when there is no in-plane Mn atom migration. However, the structure with in-plane migration (dotted circles in magenta and black arrow) is the most stable configuration. Note: we evaluated the relative energies of different configurations at a fixed hole density. Since the hole density is directly dictated by the number of Na atoms removed, we normalized the energy by “per Na removed”, thus it is the unit of the energy (**D**) The mechanism for the hole polarons. The split-polaron configuration provides a stronger screening for the long-range electrostatics between the Na vacancy sites (dotted circles in cyan) compared to the other configuration.

We note that holes on oxygen have been proposed in many systems.^{9,13,24,27,28} Intensity changes in the ~531 eV region of the O *K* edge XAS (i.e. considerably above the absorption onset) are often claimed as evidence of such species, due to presumed large shifts in core level energies arising from the reduced electron density around oxidized O1 anions compared to O²⁻. However, we have ruled out the presence of major chemical shifts (fig. S8 and the Supplementary Information for details), and show that localized hole polarons in fact manifest spectroscopically as an intensity at ~527.5 eV. We performed x-ray photoelectron spectroscopy (XPS) simulation of charged state of Na_{2-x}Mn₃O₇. The relative chemical shift of the O-*1s* core-level on O⁻ sites is estimated to be approximately 2 eV. Given that the O⁻ hole mid-gap state has a single-particle energy that is roughly 1 eV below the conduction band (CB) minimum (see Figure 3F), and taking into account an additional core-excitonic interaction of roughly 1-1.5 eV in XAS, the O⁻ *1s* → *2p* (hole) XAS transition is expected to appear as a pre-edge near ~527.5 eV to the O²⁻ *1s* → CB XAS transitions that form the main edge at 529.5 eV. Our results highlight the importance of corroborating ground state DFT calculations with explicit spectroscopic simulation. It becomes increasingly clear that unoccupied O *2p* character states can only appear far above the absorption onset at the O *K* edge (i.e. ~531 eV) due to major covalent bonding rearrangements, such as the formation of < 1.5 Å O–O dimers, which raise the energy of the non-bonding O *2p* states by forming hybridized antibonding states.^{1,7,9,10,29}

Driven by the significant covalent energy, oxygen hole polarons generally form O-O dimers.^{4,5} Previous direct detection of O⁻ species in metal oxides by electron paramagnetic resonance has been reported only at liquid-helium temperatures after irradiation or chemical doping.²⁹ Some even argued O⁻ ions with negligible covalence cannot exist as bulk oxidized species,³⁰ and indeed there have been incorrect assignments of spectroscopic signals.^{9,13,27,28} However, in Na_{2-x}Mn₃O₇ we observe the hole polaron XAS

signal in the desodiated state for at least 10 cycles (Fig. 2C). To understand the stabilization mechanism, we systematically explored different arrangements involving two oxygen holes and two Na vacancies. In addition to the 3NN arrangement already considered, we now examine the oxidation of first and second-nearest neighbor O1 (1NN and 2NN, respectively (fig. S9)). Energetic stability is referenced to the peroxo dimer configuration (Fig. 4C), though more oxidized oxygen could be more stable (which we discuss later). For the 1NN configuration, it is 0.1 eV (per Na removed) less stable than the peroxo dimer. On the other hand, the 3NN configuration - wherein the two holes are maximally separated within the vacancy center (forming a linear chain consisting of oxygen polaron - Mn vacancy and oxygen polaron) is essentially as stable as the peroxo dimer. Given the highly localized nature of the oxygen holes, the stability of the 3NN relative to 1NN and peroxo dimer is dominated by coulombic interactions. Specifically, the 3NN configuration has a higher degree of symmetry, with the positively-charged oxygen holes providing better charge screening for the negatively-charged Na vacancies (See Fig. 4D).

In our calculations, we also identified an unusual split-hole polaron configuration, where a hole is shared among two O1 atoms via a very weak covalent bond (evidenced by the long O-O distance $\sim 2.6 \text{ \AA}$, as well as by the DOS (Fig 4D, fig. S10). This species can be loosely regarded as O_2^{3-} . This is unusual because cation vacancy bound deep acceptor states in wide gap oxides typically tend to form small polarons with spin density localized on a single O^- site.³¹ We found that the split-hole configuration is the most stable: $\sim 0.23 \text{ eV}$ and $\sim 0.34 \text{ eV}$ (per Na removed) more stable than 3NN and 1NN. These energies are significantly greater than $k_{\text{B}}T$ ($\sim 0.025 \text{ eV}$). The explanation for this surprising stability (Table S1) lies in the selective removal of Na ions at the Na2 octahedral sites. Recall that Na ions at Na1 are not extracted during the 4.25 V plateau.¹⁴ The positively charged holes are bound by coulombic forces to the negatively charged Na2 vacancy site. In the case of the split-hole polaron, a hole density is shared among two oxygen atoms and the oxidized O1 comes closer to the Na vacancy than in the 3NN configuration (Fig. 4D). The energy lowering via coulombic attraction in this state comes at the cost of some electron-lattice strain energy and exchange energy which tends to favor localization on an O1 site as in the 3NN case. We note that the XAS simulation for 3NN and split oxygen-hole polarons give similar spectroscopic signatures (peak \sim

527.5 eV) (fig. S10). Therefore, we cannot distinguish the two types of polarons within our spectroscopy simulation accuracy limits. Nonetheless, both configurations are predicted to be as or more stable than the peroxy dimer, which likely explains the complete absence of the latter and the minimal hysteresis.

To confirm the crucial role of coulombic interaction in stabilizing the oxygen hole polaron, we investigated several other extent and configuration of desodiation. Even at 25% desodiation, for partially occupied Na2 vacancy arrangement, the split-hole polaron is predicted to be more stable than the localized hole by 0.3 eV (fig. S11). The situation is different, however, in the case of desodiating prismatic Na1 sites that sit on top of the Mn vacancy (fig. S12). In this case no split-hole polaron is predicted and a 3NN configuration wherein each hole localizes on an O1 site closest to one of the Na1 vacancies is stabilized (which would give rise to the same spectroscopic signature as we observe up to 4.7 V). While Na1 desodiation is overall energetically unfavorable, the hole density distribution is consistent with an electrostatically driven mechanism (fig. S12). At different states of desodiation, the Na2 vacancies can be disordered in the material and different Mn vacancy sites can locally experience variations in sodium vacancy ordering. Nevertheless, since electrostatic forces in this material favor keeping hole densities separated, the dimer configuration will continue to be relatively disfavored (Fig 4, fig S10). Even in the presence of Na2 vacancy inhomogeneity, we expect Mn vacancy sites overall to support a distribution of the split-hole and localized O⁻ hole configurations.

Recently, Bruce and colleagues suggested a new redox mechanism to describe anionic redox materials with high voltage hysteresis.^{8,9} The mechanism involves in-plane TM migration and formation of O-O dimer with a bond length of ~ 1.2 Å. We explored this possibility in 50% desodiation of Na_{2-x}Mn₃O₇ (Fig. 4C) and found that such configuration is more stable than split-hole polaron by -340 meV. This is consistent with our observation that the hole polaron XAS feature disappears after more than 2 days from electrode harvesting, fig. S13). A previous EPR study also showed that hyperfine lines, which are related to the oxidized species in charged Na_{2-x}Mn₃O₇, disappeared after 7 days, also suggesting that the paramagnetic hole polarons ultimately form a diamagnetic O-O dimer.¹⁴ These observations indicate that hole polarons in this material is metastable and could have a substantial, but finite lifetime, potentially explaining why

previous XAS reports on $\text{Na}_{2-x}\text{Mn}_3\text{O}_7$ did not observe the peak at 527.5 eV. However, we have shown that holes can reversibly dis/appear during dis/charge (Figs. 2B and 2C) for several cycles, as fresh hole polarons, created every cycle, do not dimerize on the time scale of our cycling condition ($C/20$), which is less than 48 hrs per cycle. Therefore, redox-structure decoupling and the exceptional reversibility remain possible in $\text{Na}_{2-x}\text{Mn}_3\text{O}_7$, since O-O dimers do not form during cycling, unlike other anionic redox active materials, possibly because of the effective polaron trapping and high migration barrier. We note that previous studies on this electrode material attributed both the small voltage hysteresis^{13,32,33} and the stability of O holes to hybridization^{13,33} between O $2p$ and Mn t_{2g} orbitals, but did not compare the relative energetics of O hole configurations and covalent bonded species.^{13,32,33} We assessed the strength of the π -type interactions between O $2p$ and Mn t_{2g} orbitals and found it to be too weak a factor to be the major stabilization mechanism for hole formation (that is, compared to coulombic stabilization and a kinetic barrier for O-O dimer formation), fig. S14.

Our computational and experimental spectroscopy suggests that we form localized oxygen hole polarons during anionic redox (Fig. 4A and S10). Fig S10 shows that localized hole polarons (O^-) instead of O-O dimers give rise to the spectroscopic feature we experimentally observe. The hole polaron does *not* introduce significant structural disorder (unlike O-O dimers whose short bond length $< 1.5 \text{ \AA}$ which causes significant bond strain and therefore cation disorder and large hysteresis^{1,8,9,20,21}). Figure 5 summarizes the stabilization mechanism of hole polarons in $\text{Na}_{2-x}\text{Mn}_3\text{O}_7$. First, coulombic stabilization of hole polarons by Na2 vacancies favors a split-hole configuration (Fig. 5 left). The removal of the Na ions leaves behind negatively-charged vacancies whose coulombic interaction with the holes residing on neighboring oxygen orbitals (O1) provides stabilization to the holes. The split-hole polaron configuration has a higher degree of symmetry to allow such interaction and therefore is the most stable one. Second, the ordered Mn vacancies provide a large kinetic barrier for in-plane cationic disordering (Fig. 5 right). While the hypothetical structure with O-O dimer and in-plane disorder is predicted to be more stable than split-hole polaron, we do *not* experimentally observe it as a stable state.

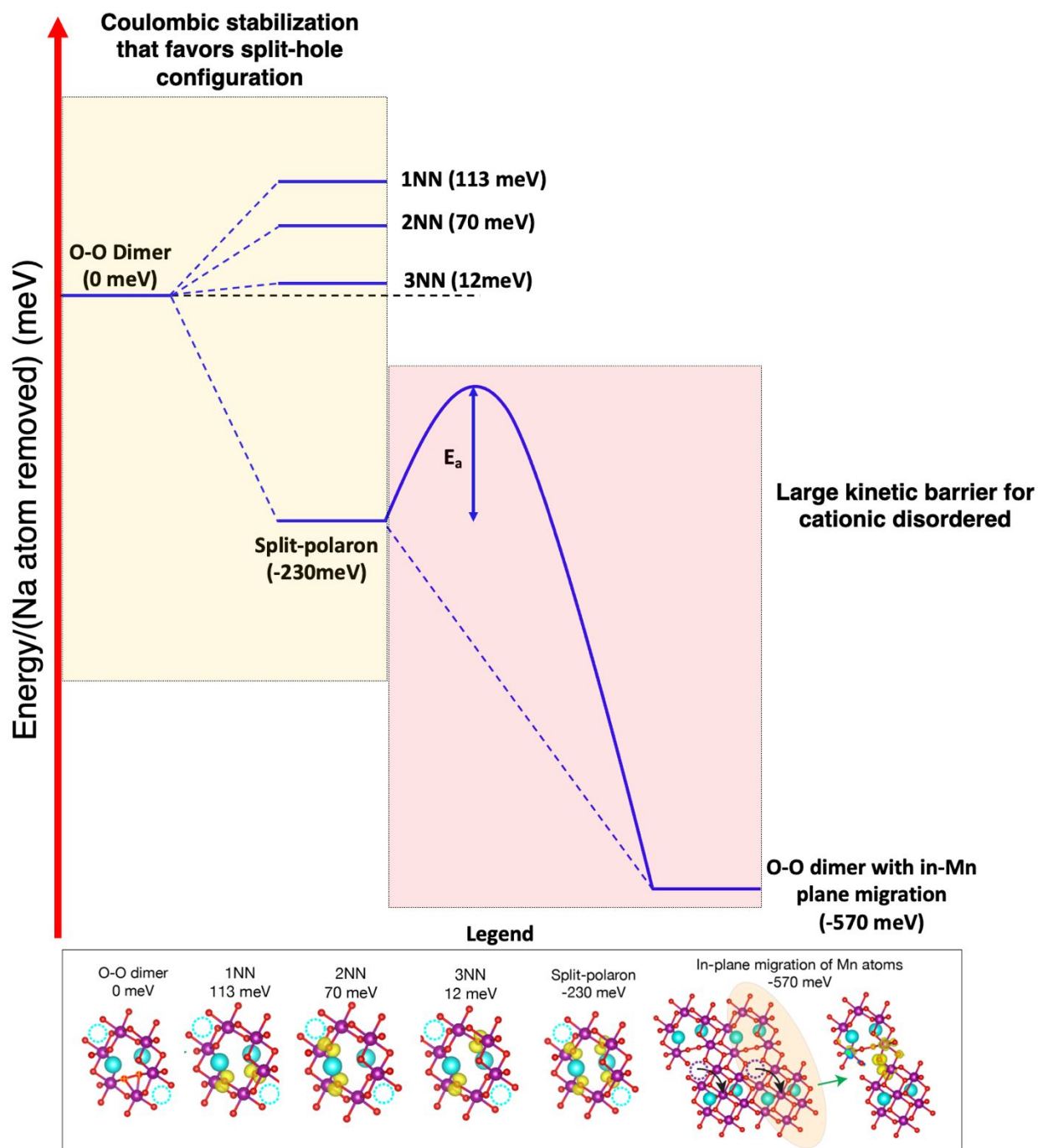


Fig.5 Coulombic stabilization and large kinetic barrier. (Left) Coulombic interactions stabilizes the split-polaron configuration over 1NN, 2NN and 3NN (NN=nearest neighbor). The split-polaron is also more stable than O-O dimers formed within the same vacancy site by ~ 230 meV (an order of magnitude higher than room temperature fluctuations, ~ 25 meV). (Right) Ordered Mn vacancies further provide a large kinetic barrier that stabilizes the split-hole polaron compared to an O-O dimer with cation disorder. The number of hop sites required for an in-plane Mn^{4+} ion to create disorder is significantly high resulting in a large kinetic barrier. Recent STEM measurements also confirmed the absence of both in-plane and out-of plane migration.³³ Future computational and experimental work investigating the migration barrier is underway in our group.

Conclusions

Design rules around high-valent redox in intercalation electrodes have evolved around tuning (1) covalent bonding and (2) local structural distortion. Our experimental and theoretical investigation of $\text{Na}_{2-x}\text{Mn}_3\text{O}_7$ show that coulombic interactions are a crucial, third contribution to the overall redox energetics. In this system, in addition to the large kinetic barrier for cation disorder, significant coulombic interactions between oxygen hole polarons and the interlayer Na vacancy which occurs over several atomic distances, is sufficiently large to disfavor O-O dimerization within individual Mn vacancy sites restricting the space of possibilities for dimer formation. These species likely dominate in the growing class of systems where cation migration is inhibited during high valent redox. Coulombic interactions also rationalize previous hypotheses and computational predictions of partially oxidized, long ($> 2 \text{ \AA}$) O-O dimers with negligible TM hybridization forming during oxygen redox.⁴ We suggest that tuning the in-plane cation-vacancy ordering, residual alkali content, and stacking order are means to control such coulombic effects. These adjust the redox chemistry and oxidized species in layered positive electrode materials to achieve O^- redox rather than O-O dimer redox and give rise to low voltage hysteresis where cation disorder/migration is suppressed. This offers the possibility to design structures to accommodate a higher hole polaron participation. The underlining principles and findings in our work can broadly be applied to other materials with in-plane transition metal (TM)-vacancy ordering. Although such ordering is naturally present in pristine $\text{Na}_2\text{Mn}_3\text{O}_7$, other materials such as $\text{Na}_{0.6}\text{Li}_{0.2}\text{Mn}_{0.8}\text{O}_2$ ⁹ display in-plane TM-vacancy ordering as the material charges, thus removing Li atoms from the transition metal layer and leaving behind in-plane ribbon ordering of TM-vacancy. $\text{Na}_{0.6}\text{Li}_{0.2}\text{Mn}_{0.8}\text{O}_2$ similarly exhibits low voltage hysteresis ($\sim 70 \text{ mV}$)⁹ and an identical spectroscopic features as $\text{Na}_2\text{Mn}_3\text{O}_7$. In summary, materials with existing TM-vacancy ordering or those developing it dynamically (after the alkali metal in the TM-layer is removed) can lead to low

hysteresis and identical spectroscopic signatures as found in this work. The general concept of employing coulombic interactions to tune high valent redox chemistry can be extended to other structural motifs such as twists³⁴ and gating.³⁵ This approach could lead to new compositions and structures with improved stability in a highly oxidized state, which has applications in energy storage and beyond such as in fuel cells, catalysis, electrochromics, memory devices and more³⁶.

Author contributions

I.I.A, W.E.G. and W.C.C. conceived the project; W.C.C., L.F.N., M.F.T and W.Y. supervised the experiments; T.P.D supervised the theoretical calculations; I.I.A and S.Y.K synthesized the materials and performed electrochemical measurements. I.I.A performed XAS, RIXS, EXAFS, Raman and XRD measurements. I.I.A, C.D.P and K.H.H. performed the theoretical calculations. I.I.A, C.D.P and S.Y.K analyzed and interpreted the data. S.S assisted in collection of XAS data. J.V. and B.M. assisted in interpreting the simulation results. I.I.A wrote the manuscript with inputs from all authors; W.C.C. directed the overall research.

Conflicts of interest

There are no conflicts of interest to declare.

Acknowledgments

The authors would like to thank Kipil Lim, Peter Csernica, Chunjing Jia, and Che-Ning Yeh for valuable discussions, and Loza Tadesse for Raman measurements. This work was supported by the U.S. Department of Energy (DOE), Office of Basic Energy Sciences, Division of Materials Sciences and Engineering (contract DE-AC02- 76SF00515). I.I.A. was additionally supported by the Stanford DARE fellowship program. W.E.G. was supported by BASF. L.F.N. would like to acknowledge NSERC for funding through their Discovery Grant platform, and the Canada Research Chair program. Use of the ALS

was supported by the Office of Science, Office of Basic Energy Sciences, of the US DOE under contract no. DE-AC02-05CH11231. Use of the SSRL, SLAC National Accelerator Laboratory, was supported by the Office of Science, Office of Basic Energy Sciences, of the US DOE under contract no. DE-AC02-76SF00515. Part of this work was performed at the Stanford Nano Shared Facilities, supported by the National Science Foundation under award ECCS-1542152. The computational work used resources at the National Energy Research Scientific Computing Center (NERSC), a U.S. DOE Office of Science User Facility operated under contract no. DE-AC02-05CH11231.

Notes and reference

1. Gent, W., Abate, I., Yang, W., Nazar, L. & Chueh, W. Design Rules for High-Valent Redox in Intercalation Electrodes. *Joule* **4**, 1369-1397 (2020)
2. Sathiya, M., Rousse, G., Ramesha, K., Laisa, C. P., Vezin, H., Sougrati, M. T., ... & Tarascon, J. M. Reversible anionic redox chemistry in high-capacity layered-oxide electrodes. *Nat. Mater.* **12**, 827–835 (2013).
3. Assat, G. & Tarascon, J.-M. Fundamental understanding and practical challenges of anionic redox activity in Li-ion batteries. *Nat. Energy* **3**, 373–386 (2018).
4. Yahia, M. B., Ben Yahia, M., Vergnet, J., Saubanère, M. & Doublet, M.-L. Unified picture of anionic redox in Li/Na-ion batteries. *Nat. Mater.* **18** 496–502 (2019).
5. Chen, H. & Islam, M. S. Lithium Extraction Mechanism in Li-Rich Li_2MnO_3 Involving Oxygen Hole Formation and Dimerization. *Chem. Mater.* **28**, 6656–6663 (2016).
6. Charles, N., Yu, Y., Giordano, L., Jung, R., Maglia, F., & Shao-Horn, Y. Toward establishing electronic and phononic signatures of reversible lattice oxygen oxidation in lithium transition metal oxides for Li-ion batteries. *Chem. Mater.* **32**, 5502–5514 (2020).
7. Hong, J., Gent, W. E., Xiao, P., Lim, K., Seo, D. H., Wu, J., ... & Chueh, W. C. Metal–oxygen decoordination stabilizes anion redox in Li-rich oxides. *Nat. Mater.* **18**, 256–265 (2019).

8. House, R. A., Rees, G. J., Pérez-Osorio, M. A., Marie, J. J., Boivin, E., Robertson, A. W., ... & Bruce, P. G. First-cycle voltage hysteresis in Li-rich 3d cathodes associated with molecular O₂ trapped in the bulk. *Nat. Energy* **5**, 777–785 (2020)
9. House, R. A., Maitra, U., Pérez-Osorio, M. A., Lozano, J. G., Jin, L., Somerville, J. W., ... & Bruce, P. G. Superstructure control of first-cycle voltage hysteresis in oxygen-redox cathodes. *Nature* **577**, 502–508 (2020).
10. Gent, W. E., Lim, K., Liang, Y., Li, Q., Barnes, T., Ahn, S. J., ... & Chueh, W. C. Coupling between oxygen redox and cation migration explains unusual electrochemistry in lithium-rich layered oxides. *Nat. Commun.* **8**, 2091 (2017).
11. Assat, G., Glazier, S. L., Delacourt, C. & Tarascon, J.-M. Probing the thermal effects of voltage hysteresis in anionic redox-based lithium-rich cathodes using isothermal calorimetry. *Nat. Energy* **4**, 647–656 (2019).
12. Eum, D., Kim, B., Kim, S. J., Park, H., Wu, J., Cho, S. P., ... & Kang, K. Voltage decay and redox asymmetry mitigation by reversible cation migration in lithium-rich layered oxide electrodes. *Nat. Mater.* **19**, 419–427 (2020).
13. Mortemard de Boisse, B., Nishimura, S. I., Watanabe, E., Lander, L., Tsuchimoto, A., Kikkawa, J., ... & Yamada, A. Highly Reversible Oxygen-Redox Chemistry at 4.1 V in Na_{4/7-x} [□_{1/7} Mn_{6/7}]O₂ (□: Mn Vacancy). *Adv. Energy Mater.* **8**, 1800409 (2018).
14. Song, B., Tang, M., Hu, E., Borkiewicz, O. J., Wiaderek, K. M., Zhang, Y., ... & Huq, A. Understanding the Low-Voltage Hysteresis of Anionic Redox in Na₂Mn₃O₇. *Chem. Mater.* **31**, 3756–3765 (2019).
15. Li, Y., Wang, X., Gao, Y., Zhang, Q., Tan, G., Kong, Q., ... & Chen, L.. Native Vacancy Enhanced Oxygen Redox Reversibility and Structural Robustness. *Adv. Energy Mater.* **9**, 1803087 (2019).
16. Adamczyk, E. & Pralong, V. Na₂Mn₃O₇: A suitable electrode material for Na-ion batteries? *Chem. Mater.* **29**, 4645–4648 (2017).

17. Assat, G., Delacourt, C., Corte, D. A. D. & Tarascon, J.-M. Editors' choice—practical assessment of anionic redox in Li-rich layered oxide cathodes: A mixed blessing for high energy Li-ion batteries. *J. Electrochem. Soc.* **163**, A2965–A2976 (2016).
18. Yabuuchi, N., Yoshida, H. & Komaba, S. Crystal Structures and Electrode Performance of Alpha-NaFeO₂ for Rechargeable Sodium Batteries. *Electrochemistry* **80**, 716–719 (2012).
19. Yabuuchi, N., Yoshii, K., Myung, S.-T., Nakai, I. & Komaba, S. Detailed studies of a high-capacity electrode material for rechargeable batteries, Li₂MnO₃-LiCo_{1/3}Ni_{1/3}Mn_{1/3}O₂. *J. Am. Chem. Soc.* **133**, 4404–4419 (2011).
20. Qiao, Y., Guo, S., Zhu, K., Liu, P., Li, X., Jiang, K., ... & Zhou, H. Reversible anionic redox activity in Na₃RuO₄ cathodes: a prototype Na-rich layered oxide. *Energy Environ. Sci.* **11**, 299–305 (2018).
21. Li, X., Qiao, Y., Guo, S., Xu, Z., Zhu, H., Zhang, X., ... & Zhou, H. Direct Visualization of the Reversible O²⁻/O⁻ Redox Process in Li-Rich Cathode Materials. *Adv. Mater.* **30**, 1705197 (2018).
22. Zhuo, Z., Liu, Y. S., Guo, J., Chuang, Y. D., Pan, F., & Yang, W.. Full energy range resonant inelastic X-ray scattering of O₂ and CO₂: Direct comparison with oxygen redox state in batteries. *J. Phys. Chem. Lett.* **11**, 2618–2623 (2020).
23. Zaanen, J., Sawatzky, G. A. & Allen, J. W. Band gaps and electronic structure of transition-metal compounds. *Phys. Rev. Lett.* **55**, 418–421 (1985).
24. Seo, D. H., Lee, J., Urban, A., Malik, R., Kang, S., & Ceder, G. The structural and chemical origin of the oxygen redox activity in layered and cation-disordered Li-excess cathode materials. *Nat. Chem.* **8**, 692–697 (2016).
25. Shirley, E. L. Theory and simulation of resonant inelastic X-ray scattering in s-p bonded systems: graphite, hexagonal boron nitride, diamond, and cubic boron nitride. *J. Electron Spectrosc.* **110–111**, 305–321 (2000).
26. Vinson, J., Jach, T., Müller, M., Unterumsberger, R. & Beckhoff, B. Quasiparticle lifetime broadening in resonant x-ray scattering of NH₄NO₃. *Phys. Rev. B* **94**, 035163 (2016).

27. Maitra, U., House, R. A., Somerville, J. W., Tapia-Ruiz, N., Lozano, J. G., Guerrini, N., ... & Bruce, P. G. Oxygen redox chemistry without excess alkali-metal ions in $\text{Na}_{2/3}[\text{Mg}_{0.28}\text{Mn}_{0.72}]\text{O}_2$. *Nat. Chem.* **10**, 288–295 (2018).
28. Luo, K., Roberts, M. R., Hao, R., Guerrini, N., Pickup, D. M., Liu, Y. S., ... & Bruce, P. G. Charge-compensation in 3d-transition-metal-oxide intercalation cathodes through the generation of localized electron holes on oxygen. *Nat. Chem.* **8**, 684–691 (2016).
29. Abate, I., Kim, S. Y., Pemmaraju, C. D., Toney, M. F., Yang, W., Devereaux, T. P., ... & Nazar, L. F. The role of metal substitution in tuning anion redox in sodium metal layered oxides revealed by X-ray spectroscopy and theory. *Angew. Chem. Int. Ed Engl.* **60**, 10880–10887 (2021).
30. Schirmer, O. F. O[−] bound small polarons in oxide materials. *J. Phys. Condens. Matter* **18**, R667 (2006).
29. Radin, M. D., Vinckeviciute, J., Seshadri, R. & Van der Ven, A. Manganese oxidation as the origin of the anomalous capacity of Mn-containing Li-excess cathode materials. *Nat. Energy* **4**, 639–646 (2019).
30. Lany, S. & Zunger, A. Polaronic hole localization and multiple hole binding of acceptors in oxide wide-gap semiconductors. *Phys. Rev. B* **80**, 085202 (2009).
33. Kitchaev, D. A., Vinckeviciute, J. & Van der Ven, A. Delocalized metal-oxygen π -redox is the origin of anomalous nonhysteretic capacity in Li-ion and Na-ion cathode materials. *J. Am. Chem. Soc.* **143**, 1908–1916 (2021).
34. Tsuchimoto, A., Shi, X. M., Kawai, K., de Boisse, B. M., Kikkawa, J., Asakura, D., ... & Yamada, A.. Nonpolarizing oxygen-redox capacity without O-O dimerization in $\text{Na}_2\text{Mn}_3\text{O}_7$. *Nat. Commun.* **12**, 631 (2021).
35. Yang, S., Prendergast, D. & Neaton, J. B. Tuning semiconductor band edge energies for solar photocatalysis via surface ligand passivation. *Nano Lett.* **12**, 383–388 (2012).
36. Ohta, T., Robinson, J. T., Feibelman, P. J., Bostwick, A., Rotenberg, E., & Beechem, T. E. Evidence for Interlayer Coupling and Moiré Periodic Potentials in Twisted Bilayer Graphene. *Phys. Rev. Lett.* **109**, 186807 (2012).

37. Sood, A., Poletayev A. D., Cogswell D. A., Csernica P. M., Mefford J. T., Fraggedakis D., Toney M. F., Lindenberg A. M., Bazant M. Z., Chueh W.C. Electrochemical ion insertion: From atoms to devices. *Nat. Rev. Mater.* 1-21 (2021).

Coulombically-stabilized oxygen hole polarons enable fully reversible oxygen redox

Iwnetim I. Abate^{1,2}, C. Das Pemmaraju², Se Young Kim³, Kuan H. Hsu¹, Sami Sainio⁴, Brian Moritz², John Vinson⁵, Michael F. Toney^{1,4}, Wanli Yang⁶, William E. Gent¹, Thomas P. Devereaux^{1,2*}, Linda F. Nazar^{3*}, William C. Chueh^{1,2}

Broader context

Increasing the energy density of battery materials is a crucial part of the global energy transition. Employing oxygen (anionic) redox in positive electrodes of lithium- and sodium-ion batteries has the potential to significantly improve their energy density by providing high voltage capacity beyond that of most transition metal redox couples. However, anionic redox typically drives rehybridization of highly oxidized oxide-anion species to form short O–O dimers, leading to structural disorder, voltage hysteresis, and voltage fade, negating much of the benefit. In this work, we report unambiguous experimental and computational spectroscopic confirmation of a redox mechanism that prevents such rehybridization and enables exceptionally low-voltage hysteresis (only 40 meV) in $\text{Na}_{2-x}\text{Mn}_3\text{O}_7$. We demonstrate that large kinetic barrier for cation migration and coulombic interactions between oxidized oxide-anions and the interlayer Na vacancies disfavor rehybridization and stabilizes hole polarons on oxygen (O^-) at 4.2 V vs. Na/Na^+ . The underlying principles and findings in our work can be applied to other materials with in-plane transition metal-vacancy ordering. This finding could lead to new compositions and structures with improved stability in a highly oxidized state, which has applications even beyond energy storage in fuel cells, catalysis, electrochromics, memory devices and more.